PAPER • **OPEN ACCESS**

Fixed type-oscillating water column front wall angle variation and impact on chamber performance: CFD numerical wave tank assessment

To cite this article: A H Samitha Weerakoon *et al* 2023 *IOP Conf. Ser.: Mater. Sci. Eng.* **1294** 012015

Fixed type-oscillating water column front wall angle variation and impact on chamber performance: CFD numerical wave tank assessment

A H Samitha Weerakoon[1,*], W Thilan, H A De Silva[2] and M Assadi[1]

[1] Faculty of Science and Technology, University of Stavanger, Stavanger, Norway
[2] Faculty of Engineering, Ocean University of Sri Lanka

* Correspondence: abeysingha.h.weerakoon@uis.no

Abstract. This study investigates optimizing the front wall geometry of an Oscillating Water Column (OWC) chamber to enhance turbine performance and output efficiency when harnessing energy from progressive waves with consistent periods and wavelengths. Numerical Wave Tank (NWT) adopted simulations carried out using ANSYS-Fluent ® package, VOF method with multiphase flow (air-water) where 2-D wave motion of NWT implemented using a C+ computer code. Frontal wall angle of the air/water chamber changed from 0° to 80°, for 10 cases. OWC system was most effective in harnessing and converting wave energy at 0° angle, reaching the maximum power output of 605.08 W/m. In contrast, 80° angle exhibited lower efficiency, with the lowest power output of 26.55 W/m. The average power output over time reflects consistent energy conversion, with the 0° angle demonstrating the highest average power output of 123.72 W/m, while the 80° case exhibited less efficient pneumatic power potential with an average of 3.5 W/m. A uniform cross section provides higher pneumatic power when with PTO in OWC. The efficiency of power generation can be increased by approximately 10 to 20% by keeping 0 to 10° angle of front wall without any appendages fitted with into the wall.

1. Introduction

The utilization of ocean waves as a renewable energy resource has gained considerable attention due to its potential to contribute to global energy demands while reducing carbon emissions [1]. The increasing demand for clean and sustainable energy sources has fueled research and development in the field of wave energy conversion. Ocean waves, a vast and virtually untapped resource, possess significant potential to meet a portion of the world's energy needs [2]. Mainly WECs can be categorized into four main types: Oscillating Water Column (OWC), overtopping systems, attenuators, and point absorbers. Among these, the OWC stands out for its advantages, including low environmental impact and minimal maintenance requirements.

The OWC concept stands out as a promising technology due to its inherent simplicity, reliability, and environmental compatibility. Among the various technologies available for harnessing wave power, the OWC concept has emerged as a promising solution [3]. The most extensively studied and successful wave energy converter (WEC) concept appears to be the Oscillating Water Column (OWC) technology, which has progressed to deploying full-scale prototypes in open sea conditions [3-5]. Japan and Europe regions commercialized floating and fixed type OWC devices as early as 1965, and more recent efforts in Ireland involved testing a 1:4th-scale buoy converter [6]. Fixed OWC devices are typically deployed

near the shore in shallow waters, which have lower wave energy compared to offshore areas due to energy dissipation from bottom friction and wave breaking, similar to small scale WEC's [7]. OWCs are celebrated for their elegant and straightforward design and operational principles. They have been implemented in various locations, including Tofteshallen, Norway (500 kW); Sakata, Japan (60 kW); Pico, Portugal (400 kW); Limpet, Scotland (500 kW); and Mutriku, Spain (300 kW), showcasing their versatility and potential for widespread use [8]. From the early days of Fixed type OWCs deployed near the shoreline to the recent emergence of floating OWCs in deeper waters and open seas. This shift towards floating OWCs is driven by the desire to tap into the immense wave energy available in these environments and to significantly scale up wave energy production. However, floating OWCs introduce intricate hydrodynamic interactions which are unbearable and extremely catastrophic under storms and high wave conditions. When waves encounter a floating OWC, they can be partially reflected, partially transmitted beneath the OWC, and partially captured by it.

Simultaneously, the incoming waves stimulate motion responses in the OWC, effectively transforming it into a wave generator that radiates waves in both seaward and leeward directions [9]. Several esteemed researchers, including Hong et al., Sphaier et al. (2010), Sykes et al., (2012) Toyota et al., (2015) and Sheng et al., (2016) have conducted extensive studies and simulations to delve into these complex hydrodynamic phenomena, striving to comprehend the behavior of floating OWCs and optimize their design [10]. Their work has led to valuable insights into factors such as heavy motion resonance, water column motion, and the damping coefficients that govern the performance of these innovative wave energy converters [9-11]. But the floating OWC structures are still considered to be not economically feasible and reliable with hash oceanic nature. However, selecting areas with locally concentrated wave energy due to topography can mitigate this issue [12]. Near-shore OWCs benefit from less exposure to harsh open-ocean wave conditions, such as seen with tidal energy conversion systems, making them more easily monitored and maintained, thus increasing their survivability [13]. Moreover, OWCs embedded in breakwaters or piers can serve dual functions, both generating energy and providing coastal protection [14], making them attractive for investment.

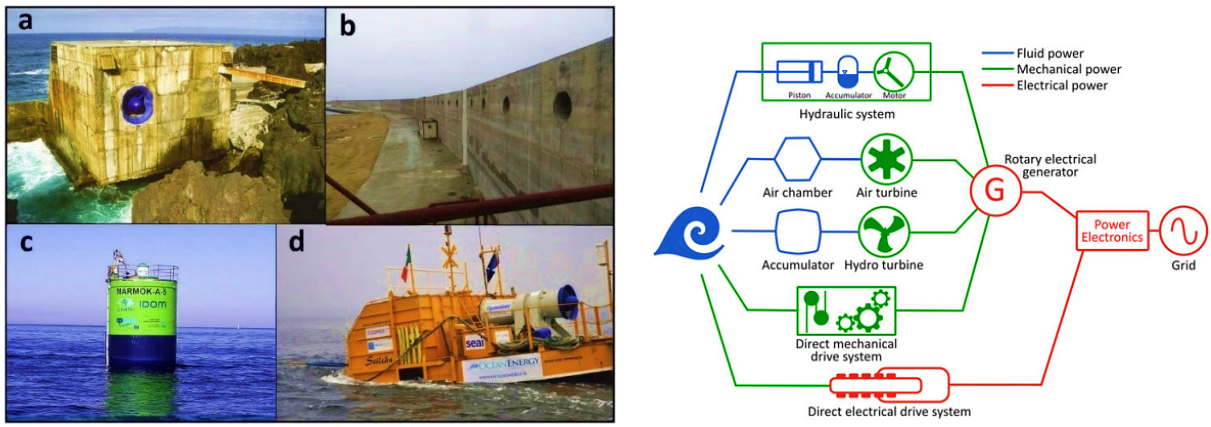

(i) **(ii)**

Figure 1. (i) OWC concepts into the sea: (a) shoreline (Pico Island, Portugal), (b) U-OWCs integrated into breakwater (Civitavecchia, Italy), (c) spar-buoy (Basque Country, Spain) (courtesy of IDOM), (d) backward-bent-duct-buoy BBDB (Galway Bay, Ireland) (courtesy of Kymaner) and (ii) Different paths for Power Take Off (PTO) from wave energy to electricity conversion [8-14]

An essential element in the makeup of wave energy converters (WECs), influencing the technical and economic effectiveness of WECs, is the power take-off (PTO) mechanism. This subsystem within WECs transforms the hydrodynamic forces acting on the WEC into valuable mechanical and usually electrical power. Diverse varieties of PTO systems are in existence, and the selection of a specific PTO for a given wave energy converter is frequently closely associated with the converter's type. The various

primary routes for converting wave energy into electricity are depicted in Figure 1 (b). The classifications of PTO systems fall into five primary groups, each of which can be studied with available published materials Ref. [10-15]. And to perceive the aim and objectives of this present study detailed descriptions of PTO methods are omitted.

The fundamental principle of OWC wave energy converters revolves around the utilization of the periodic motion of ocean waves. The OWC device consists of a collector chamber, designed to extract power from the incoming waves. As waves impinge upon the front wall of the chamber, the air trapped inside undergoes oscillatory motion, resulting in pressure variations [15]. The simple form (Figure 2, provide a visual representation of how this technology harnesses wave energy to generate electricity) of OWC consists of a chamber with an "air turbine" (mainly the *wells turbine*) positioned on top of the structure. The lower part of the chamber is open to the sea, allowing waves to enter. When waves interact with the chamber, they cause the water inside to oscillate. This oscillation, in turn, pushes and pulls air through the connected air turbine and into the atmosphere. Remarkably, the turbine rotates in a consistent direction regardless of the airflow's direction. The OWC operates in two distinct steps: first, it transforms hydrodynamic energy into pneumatic energy within the chamber, and then it converts this pneumatic energy into electricity using the turbine. The schematic operation of an OWC is illustrated in Figure 2.

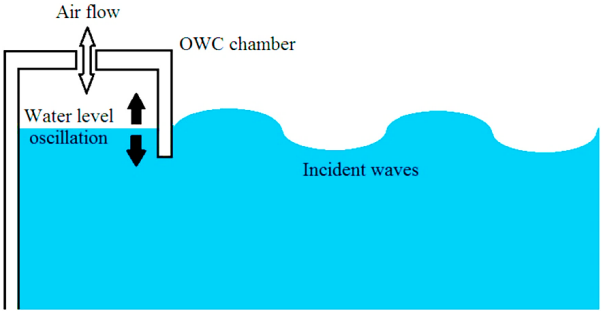

Figure 2. Fixed type OWC operation [16]

The schematic operation of an OWC is illustrated in Figure 1, providing a visual representation of how this technology harnesses wave energy to generate electricity. The pneumatic power is then converted into useful form of work through a Power Take Off (PTO) system [17]. The power train of an OWC system, which involves the conversion of wave energy into electrical energy. This process consists of several stages, first, the wave energy is transferred to the oscillating air column within the chamber and next, the energy embedded in the oscillating motion is transferred to the mechanical rotation of a turbine shaft and finally, the turbine shaft drives a generator that converts the rotation into electrical energy. The overall efficiency of an OWC system depends on the efficiencies of both the oscillating air column and the turbine itself [18-19]. Several researchers have extensively studied the impact of various bi-directional turbines on the overall operation and efficiency of OWC systems. These turbines were designed with symmetrical placement of blades, resulting in Uni-directional turbine shaft rotation. Factors such as blade arrangement, guide vanes, and non-return valves have also been subjects of research to optimize turbine efficiency [19]. Additionally, studies have explored energy dissipation and power output of turbines under different air flow conditions with a fixed chamber geometry [20].

1.1 Geometric optimization and output efficiency of OWC chamber

The geometric optimization of an OWC chamber plays a crucial role in maximizing wave energy capture and enhancing the efficiency of the system. This process involves designing the chamber shape, size, and turbine placement to optimize the oscillation of the air column and increase the overall power generation. One of the key parameters in the geometric optimization is the chamber length (l). The length of the chamber affects the wave propagation inside it and the resulting oscillation of the water column. Longer chambers allow for more wave interaction, increasing the energy capture potential.

However, there is an optimal length that balances wave energy extraction and excessive energy loss due to wave reflection. Determining this optimal chamber length involves considering factors such as wave characteristics, site-specific conditions, and the desired power output [8, 15]. The chamber width (b) is another important parameter in geometric optimization. Wider chambers provide a larger surface area for wave interaction, allowing for more efficient energy capture. However, excessively wide chambers can lead to increased wave reflection, resulting in energy losses. Thus, optimizing the chamber width involves finding a balance between maximizing energy capture and minimizing wave reflection [10, 17]. The height of the chamber (h) is also a crucial factor to consider. The height determines the volume of the air column and influences the magnitude of air compression and expansion during wave oscillation. A larger air column volume can result in higher air pressures and increased turbine performance. However, it is essential to ensure that the chamber height is within practical limits and feasible for construction and maintenance purposes [16-20].

The position of the turbine inside the chamber is another aspect of geometric optimization. Placing the turbine at the optimal location within the chamber is vital for efficient energy conversion. The turbine should be positioned to capture the maximum airflow generated by the OWC. Computational fluid dynamics (CFD) simulations and experimental studies are often employed to determine the optimal turbine placement. But in this study the CFD method is involved for the frontal wall shape optimization [7, 15-17]. In addition to the shape and size parameters, the overall chamber geometry needs to be optimized to enhance wave focusing and energy capture. Various chamber shapes, such as converging or concave designs and front wall optimization of the chamber have been studied to exploit the wave energy focusing effect. These shapes can help concentrate the wave energy towards the air column, increasing the power output. The optimization process considers factors like wave diffraction, wave reflection, and the desired energy conversion efficiency to determine the most suitable chamber shape [19-21].

1.2 Front wall angle variation and output efficiency of OWC chamber

The output efficiency of an OWC chamber is a vital performance parameter directly impacting the overall energy conversion efficiency [18]. It represents the ratio of electrical power output to the wave energy input. Several factors influence this efficiency:

- *Turbine Performance*: The efficiency of the turbine in converting air column kinetic energy into electrical power significantly affects output efficiency. Choosing an efficient turbine type and optimizing its design and operation can enhance the system's efficiency [19].
- *Geometric Design*: Optimizing the OWC chamber's dimensions, like length, width, and height, is crucial. Balancing wave energy capture and minimizing losses due to reflections and dissipation within the chamber is key. Geometric optimization improves energy extraction from incident waves [20].
- *Wave Characteristics*: Local wave conditions, including height, period, and direction, influence the energy content and the ability to induce efficient air column oscillation. Understanding and analyzing the wave climate through measurements and modeling is essential for optimizing output efficiency [21].
- *Generator Efficiency*: The electrical generator's efficiency in converting mechanical power from the turbine affects overall efficiency. Higher generator efficiency reduces energy loss during conversion [22].

Enhancing output efficiency requires a comprehensive approach, considering turbine, chamber design, wave characteristics, and generator efficiency. Optimizing these factors individually and ensuring their compatibility can lead to significant improvements. Real-world challenges such as varying wave conditions, operational limitations, and maintenance requirements must be considered.

Ongoing research in turbine design, chamber optimization, and system integration advances the state-of-the-art, improving practical OWC applications. Improving OWC system output efficiency is crucial for making wave energy economically viable and competitive as a renewable energy source. Maximizing energy conversion efficiency allows OWC technologies to better contribute to the global energy transition and harness the ocean's immense power potential [20-23]. Several researchers (Table 1) have conducted numerical and experimental investigations on the geometric optimization of OWC chambers.

Table 1. Key findings on chamber geometry optimization in OWC systems

Key finding on OWC chamber performance	Study (Ref.)
Numerical simulation of an oscillating water column device and investigating the effects of lip submergence on velocity and pressure.	[34]
Larger chamber diameter significantly enhances turbine performance in OWC systems.	[35]
Longer chamber length and higher turbine blade pitch angle lead to higher output efficiency in OWC systems.	[36]
Extending chamber length and reducing inlet height positively affect OWC system efficiency.	[37]
Genetic algorithm optimization of chamber geometry improves OWC system power output by 18%.	[38]
Increasing chamber diameter results in higher power output and efficiency in OWC systems.	[39]
Enlarging chamber diameter and adjusting draft tube diameter enhance power output and efficiency.	[40]
Multi-objective genetic algorithm optimizes chamber geometry based on wave conditions and desired power output.	[41]
Vortex shedding at the sharp edge of the OWC chamber enhances the spatial non-uniformity inside the OWC chamber through a resonant sloshing mechanism	[42]
Ideal gas adiabatic polytropic process and the real gas model were observed, a new value for the polytropic exponent was proposed, representing a non–adiabatic real gas behavior for the air–water vapor mixture of OWC chamber.	[43]
Rectangular chambers and Dual-Opening chamber with large aspect ratios yield higher power output in OWC systems.	[44]
Chamber height influences power output, and thick front wall and a large incidence angle of the wave can significantly narrow the hydrodynamic efficiency band and modify the resonant frequency in higher power generation.	[45]
A parabolic chamber shape with a specific height-to-length ratio maximizes power output, propose OWC numerical analysis for modified upper OWC chamber shape and four vertical plates inside the chamber and signify the improved peak efficiency.	[46]

While numerous OWC fixed type models and prototypes for harnessing ocean wave energy have been developed over many decades, achieving consensus on an economically competitive and reliable design remains a challenge [21-22]. The best method many researchers have focused with development is using Computational Fluid Dynamics (CFD) technology for optimization of OWC systems. Not only the CFD based Finite Volume Method (FVM) approaches developed, but also, studies concentration OWC optimization and design, several studies gained efforts related to the hydrodynamic properties and

performance evaluation of OWC wave power devices, particularly within the context of numerical simulations and experiments [22-23]. Some key methods and approaches include: -

- *Linear Theory Analysis* by Hong et al. [6]: They presented numerical estimations of hydrodynamic properties for a floating OWC device using linear theory.
- *Optimal Moonpool Geometry* by Sphaier et al. [7]: Their experimental study aimed to find the optimal entrance geometry of a moonpool to minimize vertical water motion during waves, revealing resonant periods and their impact.
- *BEM Code Predictions* by Sykes et al. [8]: They employed a Boundary Element Method (BEM) code to predict the displacement and hydrodynamic properties of a floating undamped OWC, comparing results with experiments.
- *Time-Domain Numerical Method* by Toyota et al. [9]: They developed a time-domain numerical method to evaluate the performance of floating OWC-type wave energy converters, considering various factors simultaneously, and found good agreement with experimental results.
- *Hydrodynamic Studies and Damping Coefficients* by Sheng et al. [10,11]: Their studies involved experimental and numerical investigations of moored floating OWCs, including tuning damping coefficients and assessing hydrodynamic performance.
- *Numerical Wave Tanks* by Repalle et al. [12] and Horko [13]: They used commercial software to simulate wave run-up and OWC system behavior, respectively, in lieu of physical wave tank experiments.
- *CFD Simulations* by various authors: Multiple studies (Marjani et al. [14], Liu et al. [15], Finnegan and Goggins [16], Teixeira [1], Falcão [17]) utilized CFD-based numerical simulations to investigate wave elevation, pressure variation, air flow, and turbine optimization for floating OWCs.
- *Simplified Time-Domain Model* by Iturrioz [18]: They presented a time-domain model for a fixed detached OWC device, aiming to develop a foundation for modeling more complex floating multi-chamber OWCs.

In this research, CFD Fixed type OWC case study employs a 2D fully nonlinear Numerical Wave Tank (NWT) based on first principles and adopting several techniques in Table 01 and hydrodynamic theories developed for OWC structure analysis. This 2-D NWT is used to analyze 2nd order, linear wave system was implemented in OWCs. Ansys ® FLUENT v19.1 software employed to solve Navier-Stokes equations and equations of motion in a coupled manner, enabling the simulation of chamber motion in response to waves. This advanced tool serves as a digital laboratory for studying the intricate interactions between waves and chamber walls of OWCs. The use of dynamic mesh simulations enhances the accuracy of the analysis, offering valuable insights into the complex dynamics at play in these energy conversion systems. This paper presents a comprehensive investigation into the performance variation of an OWC wave energy converter by optimizing the front wall configuration and providing insights into the power development potential of the OWC structure.

2. Methodology

2.1 Case Study Theories: Fixed type OWC, NWT and Ocean Wave Mechanics

2.1.1 Formulating wave parameters and chamber design. The OWC chamber designed adopting case study by Falcão [24] the dimensions ratios and OWC structure is then matched for the present case study. As shown in the Figure 3, the OWC hypothetical case considered. A fixed-structure OWC considered where, the water depth is h. In calm water, the submerged potion taken as b. The thickness of the walls is assumed negligible.

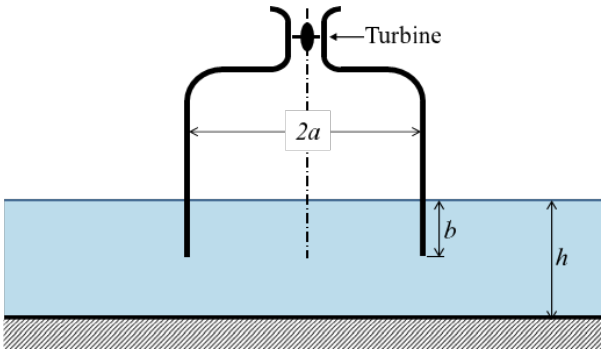

Figure 3. Fixed-OWC hypothetical structure [24]

The dimensionless hydrodynamic coefficients G* (radiation conductance) and H* (radiation susceptance) are defined as,

$$\{G^*, H^*\} = \frac{\rho_w g}{\omega \pi a^2}\{G, H\} \quad (1)$$

Where ρ_w is the water density, g is the acceleration of gravity and $\boldsymbol{\omega}$ is the wave radian frequency. For an axisymmetric OWC, the excitation flow rate coefficient $\boldsymbol{\tau}$ is related to G by (Ref. [25-26])

$$\tau = \left[\frac{2\rho_w g^2 D(kh) G}{\omega k}\right]^{1/2} \quad (2)$$

where *k* is the wavenumber and

$$D(kh) = \left[1 + \frac{2kh}{\sinh 2kh}\right] \tanh kh \quad (3)$$

which may be written in dimensionless form as

$$\tau^* = \left[\frac{2\pi D(kh) G^*}{a^* kh}\right] \quad (4)$$

where $\tau^* = g^{-1/2} a^{-3/2} \tau$ and $a^* = a/h$. In the equations above, kh need to be expressed as $kh = \omega^* c^* \sqrt{a^*}$ where $\omega^* = \omega\sqrt{a/g}$ is the dimensionless wave frequency, and dimensionless wave celerity $c^* = c/\sqrt{gh}$ is the solution of the dispersion relationship in finding the wave speed matching with the case study.

$$c^* = \frac{\sqrt{a^*}}{\omega^*} tanh \frac{\omega^*}{c^* a^*} \quad (5)$$

To use the wave celerity value from Eq. 05, specifically for the simulation purposes, we use the Stokes 2nd order wave theory. Where upstream wave amplitude and wavelength corresponding to the second-order Strokes theory, we therefore impose the velocity components provided as boundary conditions on the numerical wave wavemaker. The wave characteristics are chosen, and it is well represented by Stokes second order solution. Difference regions of validity for various theories are described by Mehaute et al., [25]. The wave considered in this study has a constant period T, wavelength λ and incoming wave height H (in Figure 4).

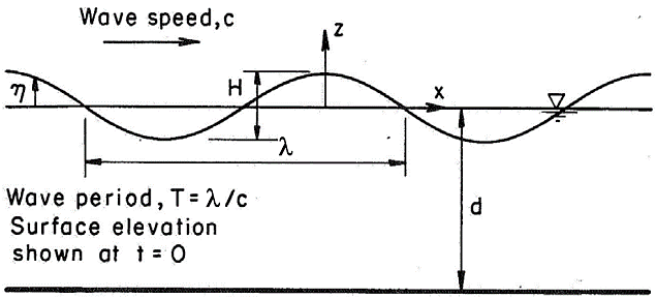

Figure 4. Defined properties of surface wave model (adopted from [27])

According to the second order theory, the equation of the free surface elevation by Dean et al., [25,26] is given as

$$\eta = \frac{H}{2} cos(kx - \omega t) + \frac{\pi H^2}{8\lambda} \frac{cosh(kh)}{sinh^3(kh)} [2 + cosh(2kh)\} cos\,(2kx - 2\omega t) \tag{6}$$

Where *t* is the time, *h* the water depth, *k* the wave number and ω is the angular frequency same as used before. The following relations give the horizontal component u and the vertical component w of the local fluid velocity:

$$\mathrm{u} = \frac{Hgk}{2\omega} \frac{cosh\, k(z+h)}{cosh(kh)} cos(kx - wt) + \frac{3H^2\omega k}{16} \frac{cosh\, 2k(h+z)}{sinh^4(kh)} cos\, 2(kx - \omega t) \tag{7}$$

$$w = \frac{Hgk}{2\omega} \frac{sinh\, k(z+h)}{cosh(kh)} sin(kx - wt) + \frac{3H^2\omega k}{16} \frac{sinh\, 2k(h+z)}{sinh^4(kh)} cos\, 2(kx - \omega t) \tag{8}$$

The dispersion relation is given by:

$$\lambda = \frac{gT^2}{2\pi} tanh\,(\frac{2\pi h}{\lambda}) \tag{9}$$

The corresponding wave incident power [27] per unit width is:

$$P_{in} = \frac{\rho g\, \lambda}{16T} H^2 \left[1 + \frac{2kh}{sinh(2kh)}\right] [1 + \frac{9}{64} \frac{H^2}{k^4 h^6}] \tag{10}$$

Assuming that the water free surface in OWC behaves as a flat plate, the hydrodynamic power transferred to the air column inside the chamber can be determined as follows:

$$P_{hyd} = p_a b \frac{dZ_p}{dt} \tag{11}$$

Where *Pa* is the air column pressure, *b* is the size of the chamber and *Zp* is the free surface elevation inside the chamber, these parameters were defined for the ease of creating the geometry in the present work based on the Ref. [24] hypothetical case study. The OWC efficiency ε computed by the ratio of the hydrodynamic power to the incident power:

$$\varepsilon = \frac{P_{hyd}}{P_{in}} \tag{12}$$

In this case we focused on the OWC front wall chamber, in particular its immersion depth and orientation versus the flow direction. However, nine cases are to be distinguish as shown in figure. All cases are studied for a same progressive monochromatic wave that has constant height and wavelength. But for the simplicity of the waves, we use some assumptions. In this paper we used the C computer program source file to generate the required wave for the simulation. The code will be as; "X = 0.5 × 1.57 × cos (1.57 × time)" represents a cosine wave with an angular frequency of 1.57 and an amplitude

of 0.5. The angular frequency determines how quickly the wave oscillates, while the amplitude determines its maximum displacement. The wavelength (λ) of a wave is the distance between two corresponding points on the wave, such as two consecutive peaks or troughs. In this case, the wavelength can be calculated using the formula: where ω represents the angular frequency.

$$\lambda = \frac{2\pi}{\omega} \tag{13}$$

In the code, angular frequency of 1.57, the calculated wavelength is approximately 4.012 units. The amplitude (A) of a wave is the maximum displacement of any point on the wave from its equilibrium position. In the code snippet, the coefficient 0.5 in front of the cosine function represents the amplitude. Therefore, the amplitude of the wave is 0.5.

Wave generation in NWT summary

- Wavelength (λ) ≈ 4.012 units: The distance between two corresponding points on the wave.
- Amplitude (A) = 0.5: The maximum displacement of any point on the wave from its equilibrium position.
- Dynamic pressure (Pd) is a critical parameter for calculating power in fluid systems. Representing the kinetic energy per unit volume of fluid and can be determined using the equation:

$$Pd = \frac{1}{2}\rho v^2 \tag{14}$$

where ρ denotes the density of the fluid and v represents the velocity of the fluid at a specific point. This formula establishes the foundation for estimating the dynamic pressure.

2.1.2 Flow rate measurement through OWC. Accurate measurement or calculation of the flow rate is essential for determining power. Flow rate quantifies the volume of fluid passing through a given point per unit time. This thesis discusses various methods of measuring flow rate, including the use of flow meters and calculations based on flow dimensions and velocity. The units of flow rate are typically in cubic meters per second (m3/s) or relevant units.

2.1.3 Power generation potential with OWC. Once the dynamic pressure (Pd) and flow rate (Q) are determined, the power (P) can be calculated using the equation.

$$P = Pd * Q \tag{15}$$

The resulting power value is expressed in units of energy per unit time, in W/m . It is important to ensure consistency in the units used for all variables in the calculation to obtain accurate results. The flow rate (Q) can be taken using following equation:

$$\mathrm{Q} = A * v \tag{16}$$

Where A represents the area and v represents the velocity of the fluid.

2.1.4 Considerations and limitations. While the presented methodology provides a useful estimation of power, it is crucial to acknowledge certain considerations and limitations. Factors such as fluid properties, flow characteristics, and system efficiency can influence the actual power output. This paper highlights the significance of accounting for these factors and provides guidance on addressing them effectively on CFD simulation basis. The theories developed according to suit frontal wall angle alteration (from 0° to 90°), adopted by present analysis. The OWC chamber performance and chamber behaviour by Vyzikas et al. [28], where validation of commercial CFD NWT model for OWCs against experimental results produced presented and adopted. Tests include irregular and regular wave conditions for performance, fixed-OWC chamber response. The OWCs testing method without PTO highlighted the potential uses where boundary condition of absorbing sea walls. Chen. et al. [29] presented correlation study of optimal chamber width with the relative front wall draught of onshore OWC structure identified and, in this study, two-phase wave flow model (VOF-Volume of Fluid)

presented for NWT specially to be utilized in OWCs. The model helps to optimize the geometrical parameters of fixed OWC. One of the key features adopted from this study was the development of a fitting formula that describes the relationship between the optimal chamber width and the front wall draught. This formula provides a convenient and practical way to understand how the width of the OWC chamber should be adjusted in relation to the front wall draught and angle to optimize the chamber performance. Using this fitting formula significantly simplified the preliminary design process of onshore fixed OWC. This simplification saved time and resources in the design phase, making it more efficient and accessible [29].

2.2 OWC model and CFD setup (NWT-model)

The real-world wave tank models are expensive to operate and only limited access and locations available for testing with these facilities. Real world application setup combined with computationally modelled with the Numerical Wave Tank (NWT) concepts and several models were considered and referred [24-32]. The NWT was introduced with regards to the 0th angle of the wall initially, while for all other scenarios, the methodology remains the same as the 0th angle. In the initial phase, CAD modeling was performed using SolidWorks Software ®. In Figure 5, the specified dimensions of the NWT presented. The 2-D geometry was kept simple to remove uncertainties and solver mesh convergence errors with lowered mesh angle errors such as skewness angle error during solving. To facilitate the simulation process, a 2-D model was imported to ANSYS Fluent ® v19.1 and converted to ANSYS environment using Space Claim software, and from 0deg angle to 90deg angle with 10 deg, variants modeled using Space Claim package. This approach was adopted to simplify the analysis and streamline the calculations. The front wall of the chamber facing the wave geometric angle from O deg to 80 deg. Was changed and analyzed during numerical simulations to assess the pneumatic power potential variation inside the air column of OWC, illustrated in Figure 5.

Once the 2-D modelling for all 10 set angles created the NWT and OWC sections were meshed for CFD simulations. The meshing process involved generating a mesh on 2-D surface area. Mesh is mixed type tetrahedral wrapping with hexahedral dominant core. Due to highly turbulent behaviour of “Air” the hexa-core mesh helps to capture numeric properties accurately. The general sizing of the mesh set to maximum of 0.2 m, and minimum 0.005 m. These sizes can be changes with software control. However, for the near area of the column, refined the mesh with manual resized mesh 0.01m of the size of element. This finer mesh around the column allows for more accurate representation of the flow initiation and propagation behaviour in that region. And shown in Figure 6 (c) the mesh sizes made finer with sizing 0.005 m making coarse mesh. The total mesh count is 96,574 elements taken as approximately 0.1 million, which is adequate for this simulation task. Increasing the mesh would proportionately increase the computation power, capacity, solving time. To capture the wave propagation and air chamber fluid variations accurately. The dynamic mesh motion method was adopted in presenting surface waves. Figure 6 (b) presents the how the dynamic mesh in CFD simulation process contracts and retract accordingly.

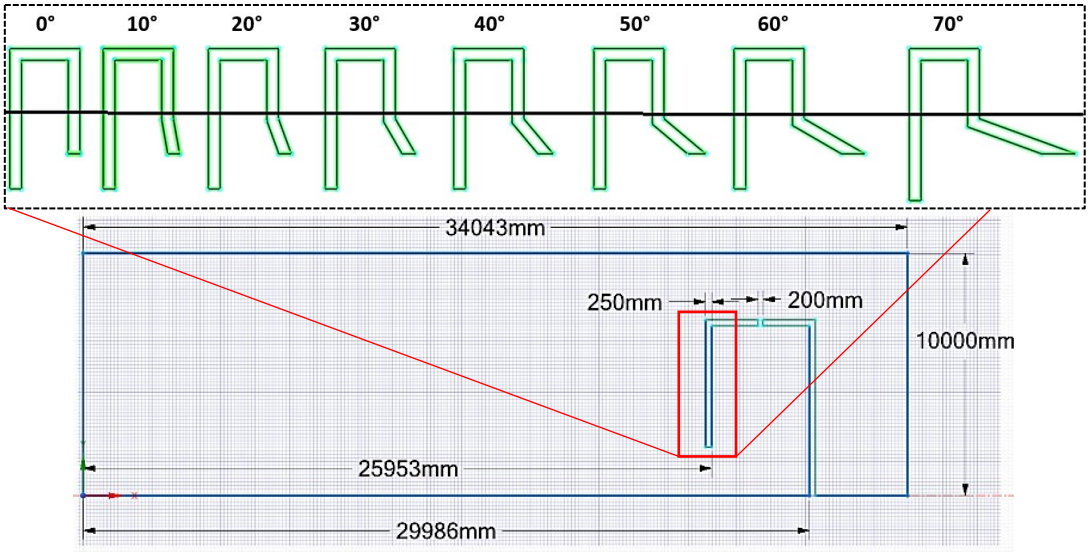

Figure 5. Geometry and dimensions of the NWT and studied OWC.

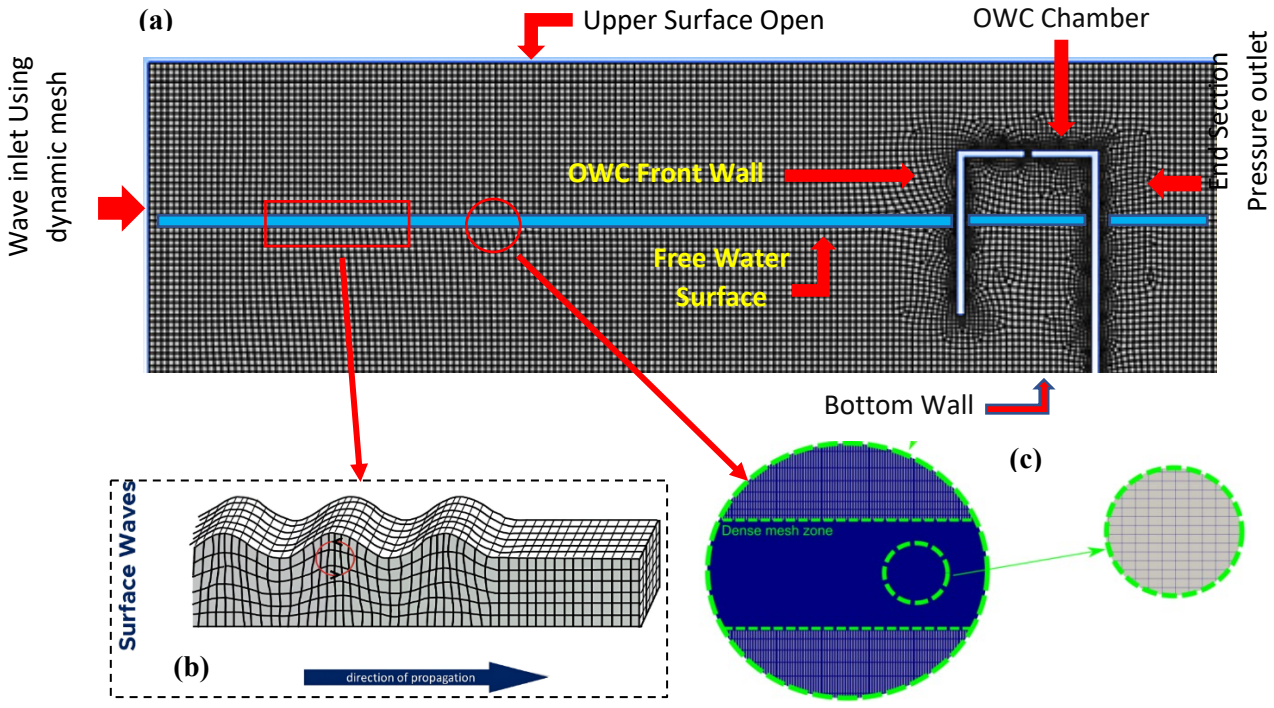

Figure 6. Computational NWT domain and the OWC chamber (a) Named sections and domain with NWT (b) Surface wave propagation model with mesh motion, and (c) The Air/Water surface denser mesh to capture accurate fluid properties.

After the mesh model created and refined with reasonable mesh quality, simulation setup using Ansys Fluent was done. The physics setup adopted the Multiphase VOF method. This model enables the simulation of flows that involve the presence of multiple fluid phases simultaneously, in this case Air being primary fluid and water secondary fluid with Volume fractions for each phase set as 0.5. The flow

modelled using RANS (Reynolds-Average Navier Stokes) equations coupled modelling. Turbulent model set as k-Omega SST model, suitable for capturing complex flow phenomena. It combines the advantages of the k-Ω (k-Omega) and k-Ɛ (k-epsilon) models to accurately predict turbulence effects in various flow conditions by switching and mixing each model near the boundaries and away from the boundaries of flow attachment. By solving equations for turbulent kinetic energy (k) and specific dissipation rate (Ω-omega), the model determines turbulence intensity (in this case 5% and 10% for wave maker and air sections) and length scales.

Ensuring accurate predictions near walls and in free shear regions. Fluid properties defined for both air and the water-liquid mixture to ensure accurate simulation of their behaviour within the system. After that, boundary conditions set as shown in Fig. o5 (A). NWT top surface was set as a pressure outlet boundary condition, whereby the solver calculates the pressure at this boundary based on flow behaviour. The wave maker uses Dynamic mesh boundary condition with C program code input for wave maker action. The outlet or end section chosen as pressure outlet wall. With viscous wave damping constant ($\beta \sim 0.087$) added. The complete numerical simulation boundary conditions, settings, mesh statistics, solver controls, convergence targets, residuals and time step settings provided with Table 2. It is important to note the Dynamic Mesh control. In a computer code developed using C language source file integrated into ANSYS Fluent, providing the necessary code to generate sinusoidal motion for the moving wall. This motion induced a wave in the liquid phase of the simulation. The source file determined motion attributes, such as amplitude and frequency.

C Code for dynamic mesh motion at the wave maker boundary to create the desired waves as follows:

```
#include "udf.h"
DEFINE_CG_MOTION (movingwall,dt,cg_vel,cg_omega,time,dtime)
{
real kecepatan_X;
real kecepatan_Y;

kecepatan_X = 0.5*1.57*cos
    (1.57*time);
kecepatan_Y = 0.0;

cg_vel[0] = kecepatan_X;
cg_vel[1] = kecepatan_Y;
cg_vel[2] = 0.0;

cg_omega[0] = 0.0;
cg_omega[1] = 0.0;
cg_omega[2] = 0.0;
```

Dynamic mesh layering was employed to allow the mesh to deform and adapt to the changing geometry during the simulation, ensuring accurate representation of fluid-structure interaction. The meshing option "cell height" was set to 0.2 m, determining cell size and aiding in controlling simulation accuracy and detail. Once the CFD setup finalized the “Initialization” carried out. Hybrid initialization used, combining the benefits of pressure-based and density-based initialization methods to establish a robust and accurate starting point for the simulation. In Figure 7(a), the final computational setup fluid domains with boundary conditions illustrated for NWT. A VOF patch operation (in Figure 7 (b)) performed during initialization to make the Ansys FLUENT solver identify Air and Water separation mesh layer easily and to aid numerical calculations making them push faster for convergence. The Mesh region dominated by hexahedral-core area illustrated in Figure 7 (c). Also, the arrows point in boundary outlet mentioning pressure outlet with relative pressure set 0 Pa.

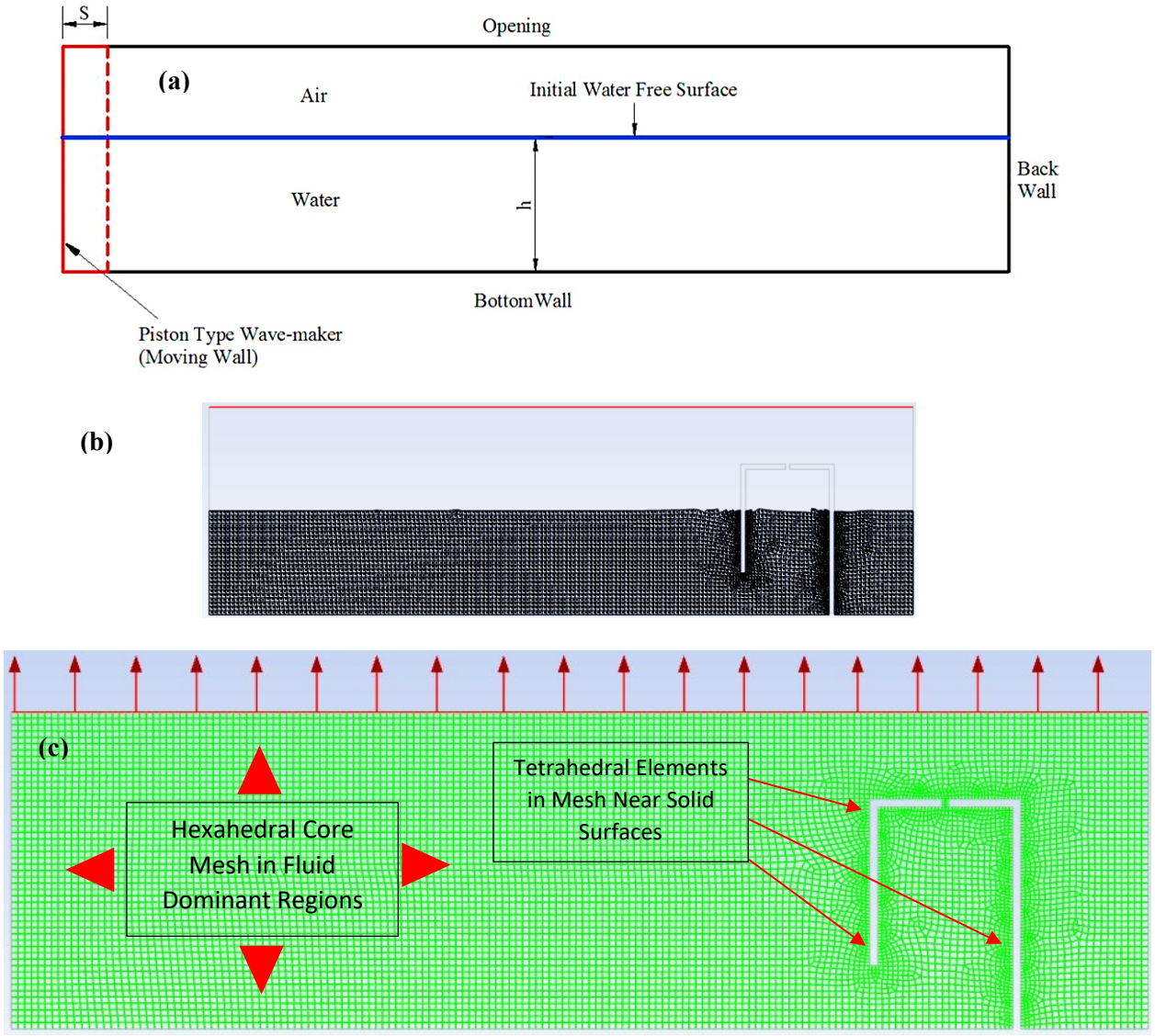

Figure 7 (a) The initialization VOF patch operation (b) Upper surface boundary condition: Pressure outlet setting and (c) the hexahedral-tetrahedral mixed but hexa-core dominant mesh model.

Table 2. Numerical simulation parameters in detail

(a) Solver	
Type	Pressure based
Velocity formulation	Absolute
Time	Transient
Simulation time	40s
Time step Size	0.05
Number of time steps	800
Iterrative loops	10
Maximum iterations	20
Convergane Target Residuals	0.0001
Simulations	1000
Iitialization	Yes

2D Space	Planar
Moving Wall	Rigid mody motion / C-Code Input
Fluid Strucuture Intercation (FSI)	ON
Gravity	Gravitational acceleration ON
Multiphase	Mixture model VOF
Fluids	Air and Water
(b) VOF Model	
VOF -Water	0.5
VOF -Air	0.5
Mixture Parameters	Slip velocity
Volume fraction parameters	Formulation - implicit
Interface modeling - type	Sharp/dispersed
Body force formulation	Implicit Body Force
Air-primary phase	Phase material - air
Water - secondary phase	Phase material - water
Phase Interaction (Air Water)	
Drag coefficient	Schiller-naumann
Slip velocity(m/s^2)	Mannninen-et-al
Surface Tention Coefficient(N/m)	Constant - 0.072
Global Options	
Surface tention force modeling	Model-continuum surface force
Viscous model	
Turbulance model	k-Omega - SST
(c) Boundary Conditions	
Top	Pressure outlet
Bottom	No-slip wall
Moving Wall	Wave maker input
Sides of NWT	Symmetry
Column	Wave maker column
Mesh type	2-D hexahedral domoinant core with Tetrahedral
Mesh Size	0.1 million (approximatly)
Type	Automatic mesh
Mesh Methods	Layering
Dynamic Mesh Zones	Moving wall - rigid body

VOF method, after initialization, produces the boundary between the air and the water surface (Air in blue and water in red). With simulation initialization 100% completed the volume fraction visually presented with Figure 8 (a). The whole idea of the NWT concept illustrated in Figure 8 (b) with the linear surface wave generated by the CFD code.

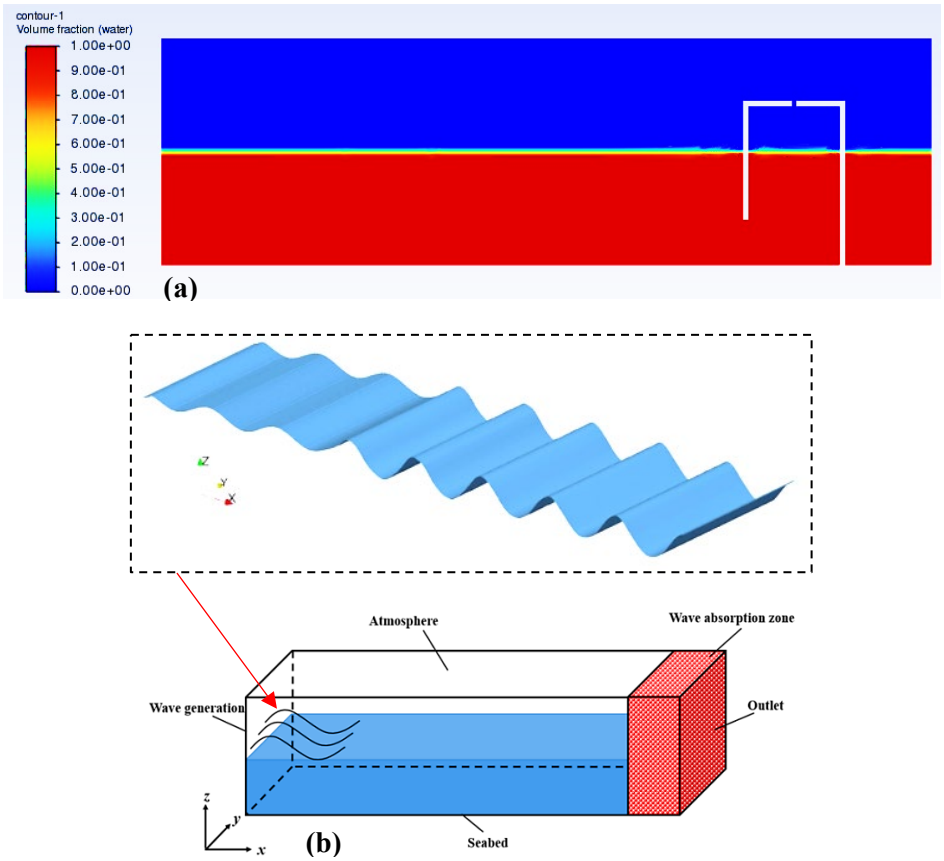

Figure 8. The Volume Fraction method defining primary fluid and secondary fluid based on Volume fraction (VF 0.5 each phase), (b) NWT operational concept with simulations.

Monitoring points implemented at a specific outlet location within the OWC chamber to track velocity and pressure values after solver finishes calculations. As shown in Figure.09 providing insights into flow behaviour at that specific point. The simulation run for 800-time steps, with each time step set at a size of 0.05. The time step size determined the temporal resolution of the simulation, influencing result accuracy and stability.

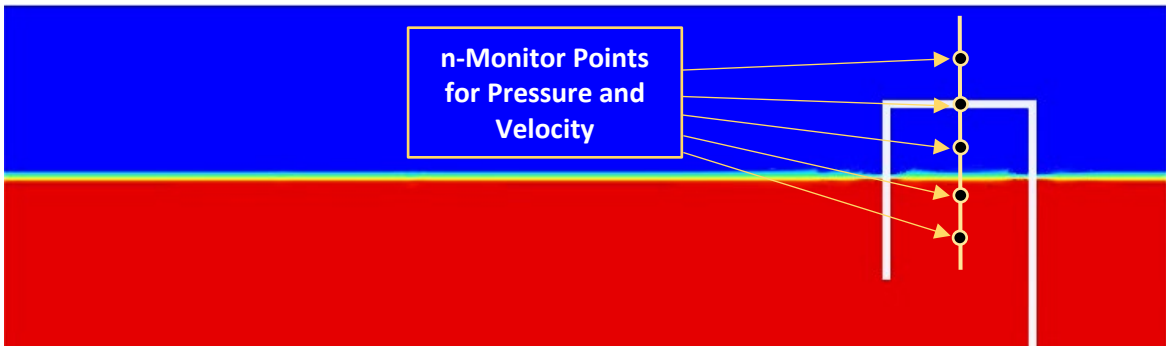

Figure 9. Monitor points (n-number) for Pressure and Velocity of OWC chamber

3. Results and discussion

3.1 Grid Independence and validation of the NWT numerical model

To validate the produced NWT model, present study was wave heights generated H (mm) was compared with the NWT model by AHS Weerakoon et al. [33] study experimental NWT model. Referring to

Figure 10 the comparison is illustrated. To assess the mesh's insensitivity within this study, the wave height profile was acquired to attain a solution that is independent of the mesh. To achieve this objective, as previously illustrated in Figure 05 and Figure 06, a fine grid is employed in the region encompassing both phases (air and water). To maintain mesh quality and ensure the grids' maximum aspect ratio remains below 20, it is necessary to reduce cell heights at the common interface between the two fluids. Various grid sizes are employed to verify the mesh independence of the numerical simulation, as demonstrated in Figure 10. In Figure 10, 'Y' represents cell heights in meters at the interface between the two phases, and experimental findings are included to validate the numerical outcomes.

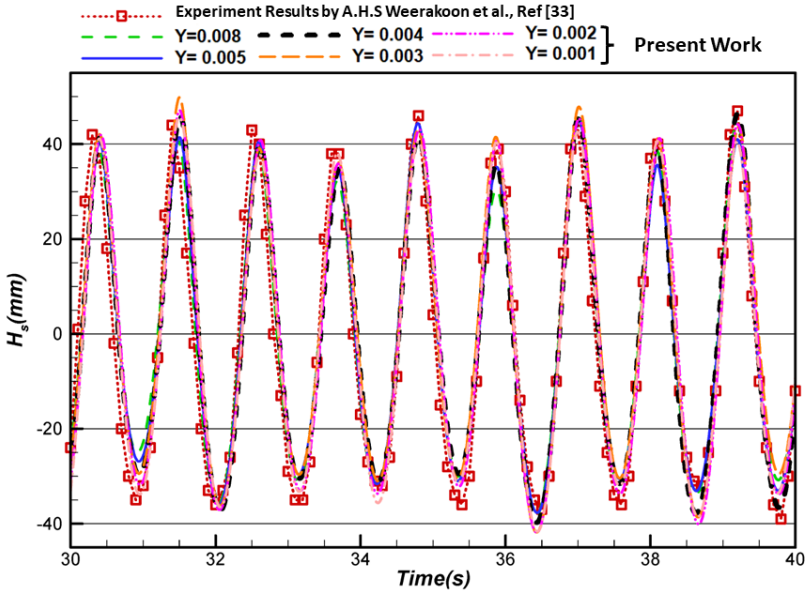

Figure 10. Validation and mesh independence of the simulation.

As indicated in Figure 10, results from cell heights below 5 mm are equivalent to *Y*=0.005 m. Consequently, reducing cell sizes below 5 mm does not alter the results but escalates computational expenses by increasing the number of grids. Figure. 11 provides the count of grids generated for different cell heights, and for the study's simulation, a grid count of 96,574 at *Y*=0.005 m is selected.

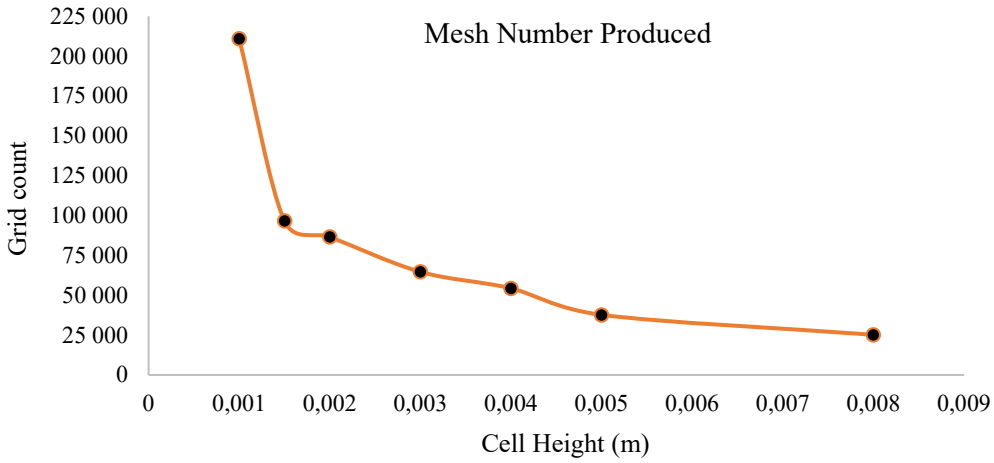

Figure 11. The number of grids produced for different cell heights.

3.2 Numerical Results with Changing the Front Wall Angle

At the end of series of simulations at each angle of front wall, pressure and velocity variations were identified. The chamber front wall being geometrically altered with 10° angle gaps starting from reference case of 0 and reaching 80. At each of these cases, average values of air velocity, ai pressure and chamber air power potential per wave meter front evaluated using CFD simulations. The wall angles from 0 to 30 divided as 1st half and 40 to 80 angle wall changes taken as 2nd half of analysis. On the 1st half (50%) of angles which provide the considerable pneumatic power potential inside the air chamber analyzed initially. At the reference case, 0º angle (vertical wall, 90° to SWL) the velocity initially experiencing a minimal increase due to slower air response inside the OWC chamber, eventually reaching 7 to 10 m/s with a sinusoidal waveform indicating successful wave energy capture. Pressure at the outlet starts low but steadily rises as wave energy accumulates, consistently staying positive (40 to 60 kPa) and peaking at 61.8 kPa. The power output per unit area initially starts low and follows a sinusoidal pattern like velocity, with a maximum of 605.08 W/m and an average of 123.72 W/m of power.

With 10º angle, velocity oscillating between positive and negative values, eventually forming a sinusoidal pattern, indicating successful wave energy capture with a maximum velocity of 8.15 m/s and an average velocity of 4.25 m/s. Examining the pressure graph (In Figure. 12. a) at the chamber outlet reveals consistently positive values, reaching a maximum of 61.8 kPa, attributed to the accumulation of wave energy within the chamber. The power output, peaking at 537.11 W/m, highlighting the impact of velocity fluctuations on power output with an average of 106.068 W/m. At 20º angle, the outlet velocity ranged from 4 to 8 m/s, reaching a maximum velocity of 7.13 m/s and an average velocity of 3.71 m/s. The pressure hits consistently positive values, peaking at 44.46 kPa, attributed to wave energy accumulation, with an average pressure of 12.43 kPa. Power output peaked 368.69W/m, concurrent with velocity fluctuations, and averaging 71.10 W/m. More opened wall at 30º angle, outlet velocity ranged between 3.71 m/s, and 6.22 m/s giving average velocity of 2.81 m/s. The pressure, peaking at 61.8 kPa, attributed to wave energy accumulation, with an average pressure of 7.25 pascals. Power output per unit area initially started low but rose over time, reaching a peak of 177.64W/m, correlated with velocity fluctuations, and averaging 32.21 W/m. The values of pressure and velocity sinusoidal variation for the 40s simulation time is illustrated in Figure 12 (a), and the chamber pneumatic power variation for 0 to 30 wall angle cases are shown in Figure 12 (b). Clear comparison is visible for each case.

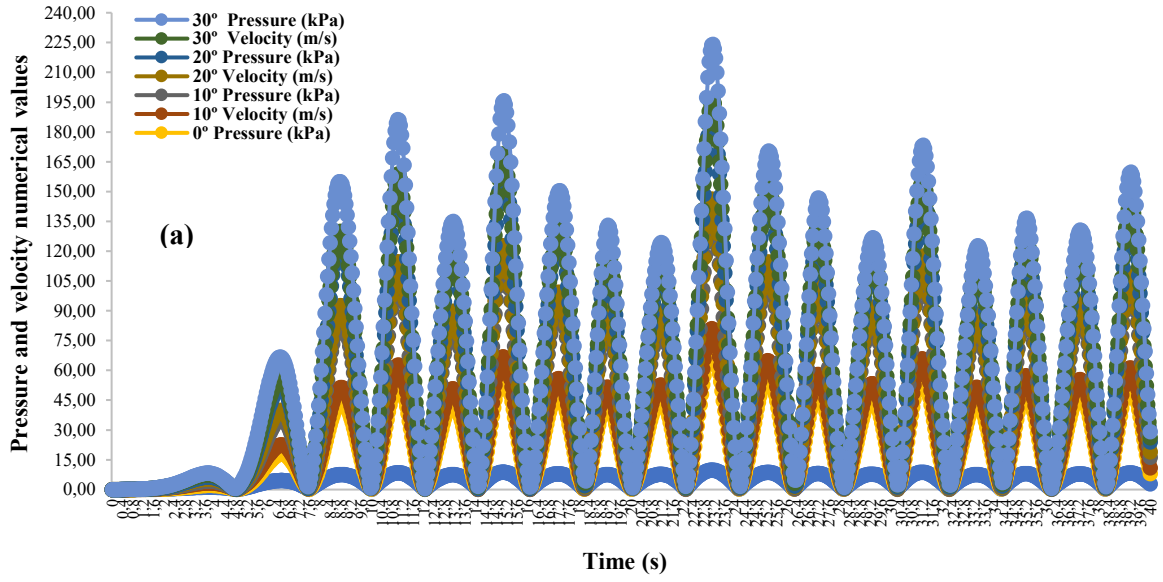

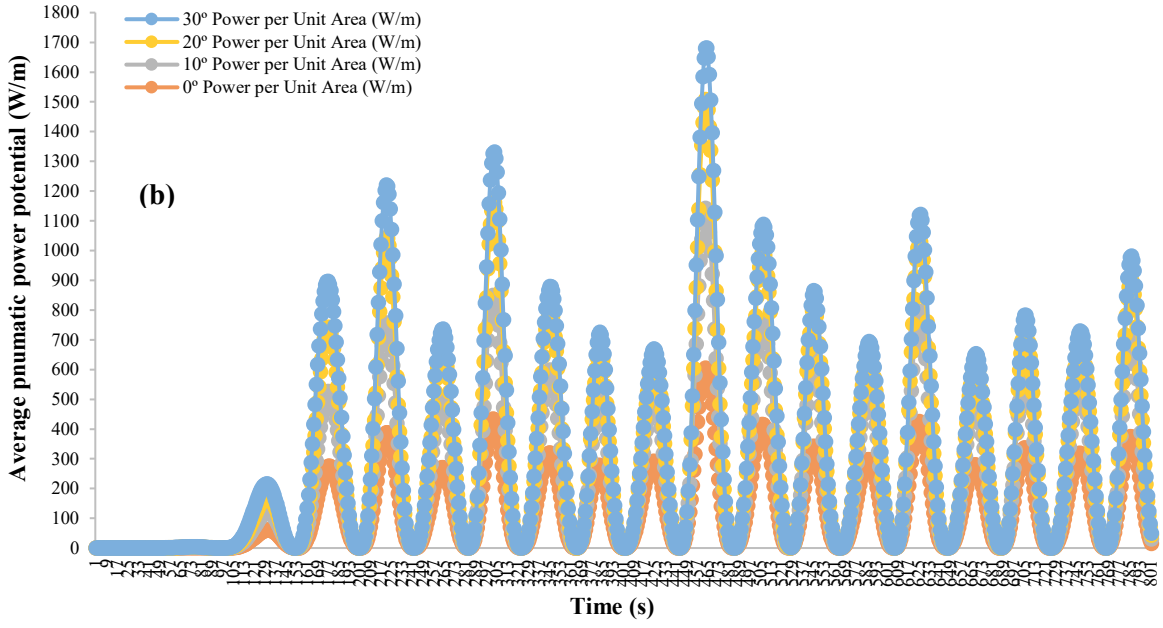

(b)

Figure 12. (a) Pressure and Velocity variations from 0º to 30º angle cases and (b) Chamber pneumatic power potential per meter of wave front in W/m

On the 2nd half (latter 50%) of wall angle cases varying from 40 to 80° can be clustered to a separate set, a contrast variation can be seen in average power values as the wall opening go pass beyond 30°. At both a 40° and 50° angle, the outlet velocity ranged from 1 to 6 m/s and 1 to 4.5 m/s, reflecting airflow dynamics and sinusoidal waveforms signifying successful wave energy capture, reaching maximum velocities of 5.33 m/s and 4.06 m/s, and average velocities of 1.59 m/s and 1.27 m/s, respectively. The pressure remained consistently positive, peaking at 61.8 kPa and 13.06 kPa, with average values of 2.56 kPa and 7.25 kPa, reflecting wave energy accumulation and efficient utilization. Power output per unit area initially started low but increased over time, peaking at 99.34W/m and 53.05W/m, with average values of 7.94 W/m and 4.16 W/m. These variations are visible in the Figure 13(a) and (b).

Simulations conducted at 60° and 70° wall angles, inside the OWC chamber, air velocities reached 4.35 m/s and 4.0 m/s, with average speeds of 2.07 m/s and 1.78 m/s. These velocities followed sinusoidal waveforms, reflecting wave energy capture and efficient utilization. Pressure values like previous cases remained consistently positive, peaking at 19.92 kPa and 15.59 kPa, with average values of 4.44 kPa and 3.11 kPa. Power output per unit area of wave front initially lower but increased with simulation time, reaching maxima of 102.73W/m and 52.38 W/m, with average values of 14.42 W/m and 8.19 W/m. In simulations at 80° velocity at the outlet ranged from approximately 0 to 2.5 m/s. The maximum velocity reached 2.34 m/s, with an average velocity of 1.07 m/s. Pressure values ranged from 1 kPa to 18 kPa with a maximum of 17.58 kPa. Power output per unit area started gave a maximum of 26.55 W/m, with an average of 3.48 W/m. These values of air velocities and pressures are illustrated in Figure 13(a) and (b) for comparison and contrast.

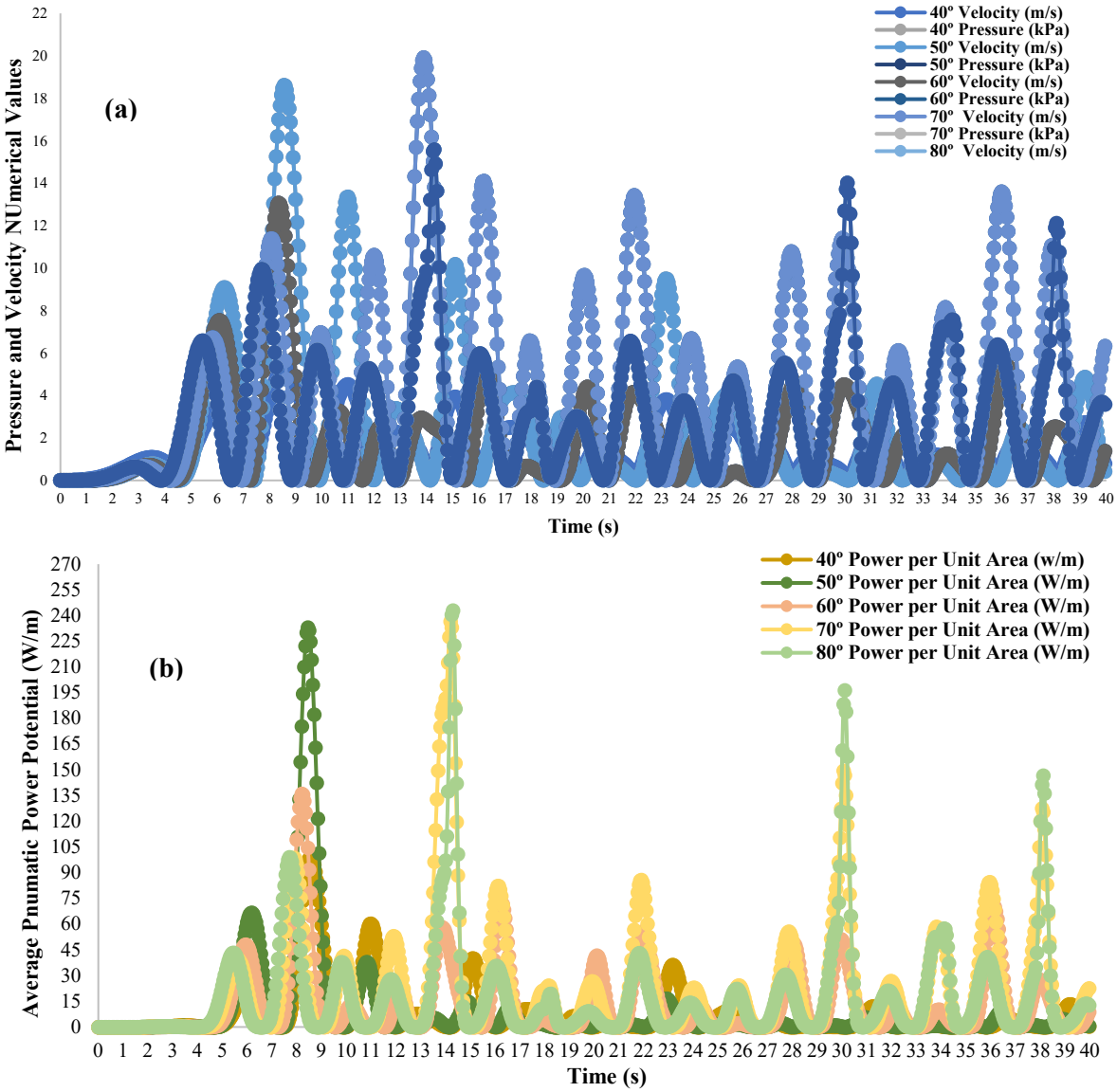

Figure 13 (a) Pressure and velocity variations from 40º to 80º angle cases and (b) Chamber pneumatic power potential per meter of wave front in W/m.

With these values the 1st 4-cases from 0 to 30° angles shown higher pressures and mainly high pneumatic power potential per unit area of wave front. Compared to the 5-case angles of 40 to 80°, which only yields considerably lower average power values. The summary of results is illustrated in Table 3. Here, the maximum values of pressures and power potentials per unit area changes did not account in summary of results. Mainly because during the simulation run, wave interference causes wave amplitude and wave lengths to superimpose, and some instances there may occur wave resonance conditions resulting extremely larger pressures and power fluctuations. To avoid these undesirable effects during analysis, the average velocities, average pressures, and average powers are illustrated in Figure 14 (a), and how the maximum velocity values varied compared to average velocities and pressures are illustrated in Figure 14 (b), for all the 9-cases.

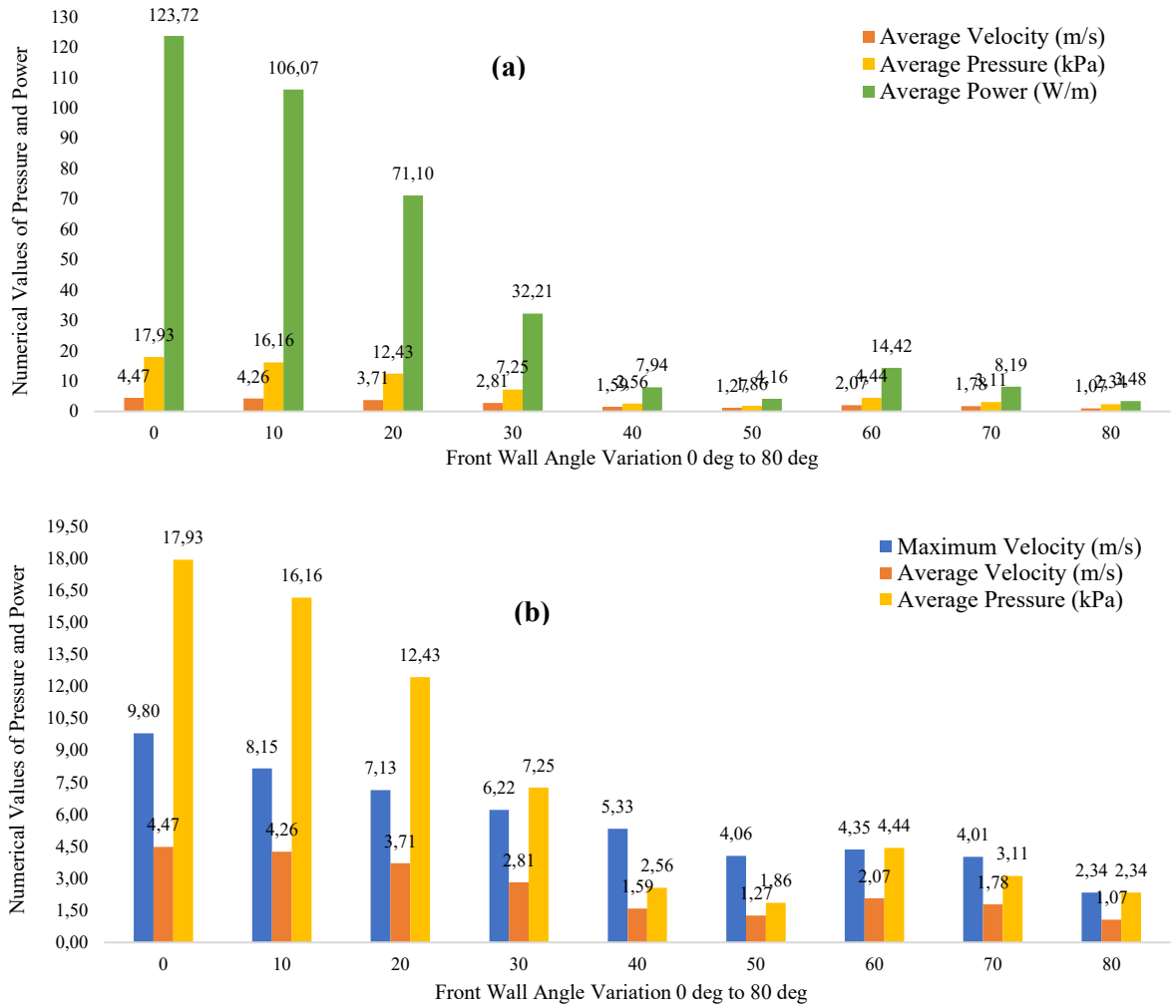

Figure 14. (a) Average pressure, velocity, and power variation inside OWC chamber for studied 9-wall angles, (b) Maximum velocity and average power and pressure variations for the 9-wall angles.

4. Conclusions

This paper presents the front wall angle variation effects on the (OWC fixed type) power potential of the air chamber. The major variation can be seen that the reference case at 0° angle produces the maximum pneumatic power potential unit are of wave front with a 123.72 W/m. And the least produced by 80° case with 3.48 W/m. A gradual power potential decrement is visible (Figure 14a) from reference wall angle to 40° angle. In between each 10° space reduction varied as 17.65, 34.97, 38.89, 24.27 and 3.77 W/m in values, in each of these stages the reduction accounts 14.27%, 39.97%, 54.7% 75.36% and 47.55% in order. Largest drop in power seen between 30 to 40° angle variation. Lowest variation seen between 0 to 10° angle locations. Beyond 30° the OWC chamber power potential diminishes exponentially and can be concluded these wall angles are not suited for OWC chamber designs, modifications, or optimization purposes. Due to wave resonance phenomena and two incident (incoming and outgoing) waves being super-positioned during collision, the chamber pressure and power potential values at 60° position reaches higher than 40 and 50° cases deviating from the pattern, and again for 70 and 80° positions these values drop with a non-linear patter which was witnessed between 0 to 50° angles.

Figure 12 illustrates the pressure and velocity variations for the 1st half (50%) of front wall angle changes are clustered. From 0º to 30º angle considered relatively smaller and the wall exerted wave

pressures are higher, due to these angles making the wall closer to normal hence the wave loading can be considerable on the wall. This causes the wave chamber pressures to increase by 20 to 30% compared to mid-span of wall angles. The highest pressures can be seen at 0° case and lowered with at 50° case, interestingly not at the 80° case, but only with a 0.2 kPa's (Figure 14 (a) and (b)). The main reason is the wave front energy being accumulated with sharp angle at 0-degree. Thus, the air chamber compressing power of the heaving motion of the wave gets increased like a liquid column entrapped pressurized in a cringer. With lower degrees of front wall angle, say the wall is perpendicular (approximately) with SWL the wave energy transferred in to the OWC chamber becomes higher, thus the compressibility increases inside a confined space facing the chamber dead wall. It is clear (In Figure. 12.b) when the chamber front wall tilted further away from the horizontal angles, the wave front energy transmitted in to the OWC chamber does not receive adequate constant cross sectional area ratio in 3-D space ($height\ x\ width\ x\ breadth$) inside the OWC air chamber because the front wall is further expanded (from 0 to 10, 20, 30…etc.) form the mean reference vertical hinge point. The pneumatic (air) power potential which works as the energy source for an air turbine, or any PTO method device, on which the useful amount of work being absorbed shows gradual decrement after 0° and further. As the front wall angle is changed it can be concluded having a constant cross section (A) to height (h) ratio is essential to increase the pneumatic (air) power potential inside the air chamber of the OWC. This condition should remain as much as possible in a uniform manner to extract useful power when an air turbine is mounted with OWC, thus the efficiency of power generation can be increased by approximately 10 to 20% with having a 0° angle of front wall without any appendages fitted with into the wall.

Funding: This project has received funding from the European Union's Horizon 2020 research and innovation program under the Marie Skłodowska-Curie grant agreement No. 861079 ("Next MGT").

Reference

[1] Zhang Y, Zhao Y, Sun W and Li J 2021 Ocean wave energy converters: Technical principle, device realization, and performance evaluation. *Renewable Sustainable Energy Rev.* **141**, 110764.
[2] Falcão A F O and Henriques J C C 2016 Oscillating-Water-Column Wave Energy Converters and Air Turbines: A Review, *Renewable Energy*, **85**, 1391-1424.
[3] Cui Y, Liu Z, Zhang X, Xu C 2019 Review of CFD Studies on Axial-Flow Self-Rectifying Turbines for OWC Wave Energy Conversion*, Ocean Eng.* **175**, 80-102.
[4] Zhou Y, Ning D, Liang D and Cai S 2021 Nonlinear Hydrodynamic Analysis of an Offshore Oscillating Water Column Wave Energy Converter, *Renewable Sustainable Energy Rev.* **145**.
[5] Doyle S and Aggidis G A 2019 Development of Multi-Oscillating Water Columns as Wave Energy Converters. *Renewable and Sustainable Energy Rev.* **107**, 75-86.
[6] Nguyen H P, Wang C M, Tay Z Y and Luong V H 2020 Wave Energy Converter and Large Floating Platform Integration: A Review. **213**.
[7] Weerakoon A H S, Kim B H, Cho Y J, Prasad D D, Ahmed M R and Lee Y H 2021 Design Optimization of a Novel Vertical Augmentation Channel Housing A Cross-Flow Turbine and Performance Evaluation as a Wave Energy Converter, *Renewable Energy*, **180**, 1300-1314.
[8] Ning D, Wang R Q, Chen L F and Sun K 2019 Experimental Investigation of a Land-Based Dual-Chamber OWC Wave Energy Converter. *Renewable and Sustainable Energy Rev.* **105**
[9] Teixeira P R F, Davyt D P, Didier E and Ramalhais R 2013 Numerical Simulation of an Oscillating Water Column Device Using a Code Based on Navier–Stokes Equations, *Energy*, **61**
[10] Hong D C, Hong S Y and Hong S W 2004 Numerical Study of the Motions and Drift Force of a Floating OWC Device, *Ocean Eng.* **31**

[11] Gomes R P F, Henriques J C C, Gato L M C and Falcão A F O 2012 Hydrodynamic Optimization of an Axisymmetric Floating Oscillating Water Column for Wave Energy Conversion, *Renewable Energy*, **44**
[12] Nunes G, Valério D, Beirão P, Sá da Costa J 2011 Modelling and Control of a Wave Energy Converter*, Renewable Energy*, **36**
[13] Mustapa M A, Yaakob O B, Ahmed Y M, Rheem C K, Koh K K and Adnan F A 2017 Wave Energy Device and Breakwater Integration: A Review. *Renewable and Sustainable Energy Rev.* **77**
[14] Weerakoon A H S, Young H S, Kim W K and Lee Y H 2020 *Novel Tidal Energy Harnessing System Utilizing Quadruple Bi-directional Turbine Arrangement*.
[15] He F and Huang Z 2014 Hydrodynamic Performance of Pile-Supported OWC-Type Structures as Breakwaters: An Experimental Study, *Ocean Eng.* **88**, 618-626.
[16] Paixão Conde J M and Gato L M C 2008 Numerical Study of the Air-Flow in an Oscillating Water Column Wave Energy Converter. *Renewable Energy*, **33**
[17] Ali T H, Nikseresht A H and Hayati M 2021 Numerical Analysis of Hydrodynamic Performance of a Dual-Chamber Oscillating Water Column, *Energy*, **221**
[18] Brito-Melo A, Gato L M C and Sarmento A J N A 2002 Analysis of Wells Turbine Design Parameters by Numerical Simulation of the OWC Performance. *Ocean Eng.* **29**
[19] Setoguchi T and Takao M 2006 Current Status of Self-Rectifying Air Turbines for Wave Energy Conversion. *Energy Conversion and Management*, **47**
[20] Weerakoon A H S, Lee Y H and Assadi M 2023 Wave Energy Convertor for Bilateral Offshore Wave Flows: A Computational Fluid Dynamics (CFD) Study. *Sustainability*
[21] Thakker A and Hourigan F 2005 Computational Fluid Dynamics Analysis of a 0.6m, 0.6 Hub-to-Tip Ratio Impulse Turbine with Fixed Guide Vanes. *Renewable Energy,* **30**
[22] Thakker A and Abdulhadi R 2008 The Performance of Wells Turbine Under Bi-directional Airflow. *Renewable Energy*, **33**
[23] Renzi, Emiliano, Michele S, Zheng S, Jin S and Greaves D 2021 Niche Applications and Flexible Devices for Wave Energy Conversion: A Review. *Energies* **14**
[24] Falcão A F O and Henriques J C C 2019 The Spring-Like Air Compressibility Effect in Oscillating-Water-Column Wave Energy Converters: Review and Analyses. *Renewable and Sustainable Energy Rev.* **112**, 483-498.
[25] Dean R G and Dalrymple R A 1991 Water Wave Mechanics for Engineers and Scientists. Advanced Series on Ocean Engineering, *World Scientific Publishing Company*.
[26] Dao B V and Penzien J 1982 Comparison of Treatments of Non-linear Drag Forces Acting on Fixed Offshore Platforms, *Appl. Ocean Res.* **4**
[27] McCormick M E 2013 Ocean Wave Energy Conversion. *Courier Corporation*.
[28] Vyzikas T, Deshoulières S, Giroux O, Barton M and Greaves D 2017 Numerical Study of Fixed Oscillating Water Column with RANS-type Two-phase CFD Model, *Renewable Energy*, **102**, Part B
[29] Chen J, Wen H, Wang Y and Wang G 2021 A Correlation Study of Optimal Chamber Width with the Relative Front Wall Draught of Onshore OWC Device, *Energy*, **225**
[30] Hayati M, Nikseresht A H and Ali T H 2020 Sequential optimization of the geometrical parameters of an OWC device based on the specific wave characteristics*, Renewable Energy,* **161**,386-394
[31] Elhanafi A, Macfarlane G, Fleming A and Leong Z 2017 Scaling and Air Compressibility Effects on a Three-dimensional Offshore Stationary OWC Wave Energy Converter. *Applied Energy*, **189**, 1-20
[32] Prasad D D, Ahmed M R, Lee Y H and Sharma R N 2017 Validation of a Piston Type Wave-maker Using Numerical Wave Tank, *Ocean Eng.* **131**, 57-67.
[33] Weerakoon A H S, Kim B H, Cho Y J, Prasad D D, Ahmed M R and Lee Y H 2021 Design Optimization of a Novel Vertical Augmentation Channel Housing a Cross-flow Turbine and

Performance Evaluation as a Wave Energy Converter, *Renewable Energy*, **180**, 1300-1314.
[34] Mohsin S I and Al-Faruk A 2021 Numerical Simulation of an Oscillating Water Column Device and Investigating the Effects of Lip Submergence on Velocity and Pressure.
[35] Mia M R, Zhao M, Wu H, Palmer H 2022 Numerical Simulation of a Stationary Offshore Multi-chamber OWC Wave Energy Converter, *Ocean Eng.* **265**
[36] Nguyen H P, Wang C M, Tay Z Y and Luong V H 2020 Wave Energy Converter and Large Floating Platform Integration: A Review. *Ocean Eng.* **21**
[37] Zheng S, Zhang Y, Iglesias G 2019 Coast/Breakwater-integrated OWC: A Theoretical Model. *Mar struct.* **66**
[38] Ning D, Zhou Y, Zhang C 2018 Hydrodynamic Modelling of a Novel Dual-chamber OWC Wave Energy Converter. *Applied Ocean Research*, **78**, 180-191
[39] Mahnamfar F, Altunkaynak A 2017 Comparison of Numerical and Experimental Analyses for Optimizing the Geometry of OWC Systems, *Ocean Eng.* **130**, 10-24.
[40] Shalby M, Elhanafi A, Walker P and Dorrell D G 2019 CFD Modelling of a Small–scale Fixed Multi–chamber OWC Device, *Applied Ocean Research*, **88**, 37-47.
[41] Bouali B and Larbi S 2017 Sequential Optimization and Performance Prediction of an Oscillating Water Column Wave Energy Converter, *Ocean Eng.* **131**, 162-173.
[42] Xu C and Huang Z 2019 Three-dimensional CFD Simulation of a Circular OWC with a Nonlinear Power-Take-off: Model Validation and a Discussion on Resonant Sloshing Inside the Pneumatic Chamber *Ocean Eng.* **176**, 184-198.
[43] Moñino A, Quirós C, Mengíbar F, Medina-Lopez E and Clavero M 2020 Thermodynamics of the OWC Chamber: Experimental Turbine Performance under Stationary Flow, *Renewable Energy*, **155**, 317-329.
[44] Wang C and Zhang Y 2022 Performance Enhancement for a Dual-chamber OWC Conceived from Side Wall Effects in Narrow Flumes, *Ocean Eng.* **247**
[45] Rodríguez A A M, Silva R C and Ilzarbe J M B 2022 The influence of oblique waves on the hydrodynamic efficiency of an onshore OWC wave energy converter, *Renewable Energy*. **183**, 687-707
[46] Kush D, Gandhi M and Banerjee 2023 Numerical Validation of Power Take-Off Damping in an OWC Chamber and Modifications for Increased Efficiency. In: Banerjee, J., Shah, R.D., Agarwal, R.K., Mitra, S. (eds) Recent Advances in Fluid Dynamics. *Lecture Notes in Mechanical Engineering*. Springer, Singapore